Variations in evapotranspiration and climate for an Amazonian semi-deciduous forest over seasonal, annual, and El Niño cycles

George L. Vourlitis, José de Souza Nogueira, Francisco de Almeida Lobo & Osvaldo Borges Pinto

International Journal of Biometeorology

ISSN 0020-7128
Volume 59
Number 2

Int J Biometeorol (2015) 59:217-230
DOI 10.1007/s00484-014-0837-1

Springer

Int J Biometeorol (2015) 59:217–230
DOI 10.1007/s00484-014-0837-1

ORIGINAL PAPER

Variations in evapotranspiration and climate for an Amazonian semi-deciduous forest over seasonal, annual, and El Niño cycles

George L. Vourlitis · José de Souza Nogueira · Francisco de Almeida Lobo · Osvaldo Borges Pinto Jr.

Received: 29 October 2013 / Revised: 9 April 2014 / Accepted: 9 April 2014 / Published online: 16 May 2014

Abstract Tropical forests exchange large amounts of water and energy with the atmosphere and are important in controlling regional and global climate; however, climate and evaportranspiration (*E*) vary significantly across multiple time scales. To better understand temporal patterns in *E* and climate, we measured the energy balance and meteorology of a semi-deciduous forest in the rainforest-savanna ecotone of northern Mato Grosso, Brazil, over a 7-year period and analyzed regional climate patterns over a 16-year period. Spectral analysis revealed that *E* and local climate exhibited consistent cycles over annual, seasonal, and weekly time scales. Annual and seasonal cycles were also apparent in the regional monthly rainfall and humidity time series, and a cycle on the order of 3–5.5 years was also apparent in the regional air temperature time series, which is coincident with the average return interval of El Niño. Annual rates of *E* were significantly affected by the 2002 El Niño. Prior to this event, annual *E* was on average 1,011 mm/year and accounted for 52 % of the annual rainfall, while after, annual *E* was 931 mm/year and accounted for 42 % of the annual rainfall. Our data also suggest that *E* declined significantly over the 7-year study period while air temperature significantly increased, which was coincident with a long-term, regional warming and drying trend. These results suggest that drought and warming induced by El Niño and/or climate change cause declines in *E* for semi-deciduous forests of the southeast Amazon Basin.

Keywords Climate change · Brazil · Deforestation · Ecotone · Energy balance · Mato Grosso · Transitional tropical forest

Electronic supplementary material The online version of this article (doi:10.1007/s00484-014-0837-1) contains supplementary material, which is available to authorized users.

G. L. Vourlitis (✉)
Biological Sciences Department, California State University, San Marcos, CA, USA
e-mail: georgev@csusm.edu

J. de Souza Nogueira · O. B. Pinto Jr.
Departamento de Física, Universidade Federal de Mato Grosso, Cuiabá, Mato Grosso, Brazil

F. de Almeida Lobo
Departamento de Solos e Engenharia Rural, Universidade Federal de Mato Grosso, Cuiabá, Mato Grosso, Brazil

Introduction

Amazonian tropical forests exchange large amounts of water and energy with the atmosphere and are important in controlling regional and global climate (Meir and Grace 2005). However, spatial and temporal variation in rainfall and dry season duration can profoundly affect energy exchange dynamics by affecting the partitioning of net radiation into sensible and latent heat exchange (Vourlitis et al. 2002, 2005, 2008; Malhi et al. 2002; da Rocha et al. 2009; Lathuilliere et al. 2012; Rodrigues et al. 2013, 2014). Forests of the northern and central Amazon Basin often exhibit little seasonal variation in evapotranspiration (*E*) because of small variation in rainfall and/or seasonal trade-offs between available energy and evaporative demand, while savanna and semi-deciduous forest of the rainforest-savanna ecotone often experience larger seasonal variation in *E* because of higher variability in rainfall and a more pronounced dry season (da Rocha et al. 2009; Vourlitis and da Rocha 2011; Rodrigues et al. 2014).

While seasonal variation in *E* has been relatively well described, interanual variations are less well known. High rainfall years also have high cloud cover (Vourlitis et al. 2011); thus, cooler-wetter years may exhibit similar rates of *E* compared to warmer-drier years. However, warming and drying that occur with El Niño (Potter et al. 2004; Malhi and

Wright 2005) can cause an increase in tree mortality (Phillips et al. 2005) that can alter C and H_2O cycling dynamics for months–years after the event (Saleska et al. 2003; Meir and Grace 2005; Qian et al. 2008; Phillips et al. 2010). Superimposed on the natural climatic variation is the climate change resulting from greenhouse gas emissions and/or land cover change, which is expected to cause a 3–5 °C increase in temperature for the Amazon Basin by the end of the twenty-first century (Cramer et al. 2005; Costa and Pires 2010). Warming and drying may be especially pronounced in areas that experience widespread deforestation because of changes in albedo, declines in surface roughness, increases in convection and runoff, and declines in soil water storage (Hodnett et al. 1995; Baidya Roy and Avissar 2002; Costa et al. 2003; Hasler and Avissar 2007; Costa and Pires 2010).

Given the potential importance of climate variation on tropical forest *E*, the goal of this research was to quantify seasonal and interannual variations in *E* and climate for a tropical semi-deciduous forest located in the rainforest-savanna ecotone of northern Mato Grosso, Brazil. This area is likely to be especially sensitive to climate variation given its transitional nature (Arris and Eagleson 1994). Here, we report temporal variations in weekly averaged *E* and local climate observed over a 7-year period and use well-known, but seldom used, spectral analyses to quantify potentially important patterns and cycles in these time series. The study period encompassed a relatively intense El Niño event in 2002 (Chen et al. 2010) and a significant drought event in 2005 (Marengo et al. 2008), allowing the characterization of *E* before and after these climate perturbations. In addition to the 7-year time series for *E* and local climate, monthly climate data was compiled for the period between 1989 and 2005 for several locales within, or adjacent to, the forest-savanna transition of northern Mato Grosso to assess longer-term, regional cycles and trends in climate. Given that over 35 % of the semi-deciduous forest of the forest-savanna ecotone of northern Mato Grosso has been converted to pasture or agriculture over the last 30 years (Soares-Filho et al. 2006), these climate data provide an opportunity to analyze if changes in climate for this climatically sensitive ecotone have changed in a manner that is consistent with what is expected from land cover change.

Material and methods

Site description

Tower-based eddy covariance was used to measure instantaneous (30 min average) rates of evapotranspiration (*E*) between January 2000 and 2007. Measurements were made in a 25–28-m-tall intact, mature *terra firme* tropical semi-deciduous forest located 50 km NE of Sinop Mato Grosso, Brazil (11° 24.75′ S: 55° 19.50′ W), 423 m above sea level (Fig. 1). Mean annual temperature is 24 °C with little seasonal variation, and rainfall is on average 2,000 mm/year with a 4–5-month dry season in May–September (Vourlitis et al. 2005). Tree species at our study site are typical of semi-deciduous Amazonian forest (Ackerly et al. 1989; Lorenzi 2000, 2002) and include *Protium sagotianum* Marchland, *Dialium guianense* (Aubl.) Sandwith, *Hevea brasiliensis* Müll. Arg., *Brosimum lactescens* (S. Moore) C.C. Berg, *Cordia alliodora* (Ruiz & Pav.) Oken, *Tovomita schomburgkii* Planch & Triana, and *Qualea paraensis* Ducke. There are approximately 80 species and 35 families of trees with a diameter ≥10 cm; however, nearly 50 % of all individuals are in the Burseraceae (*P. sagotianum*), Clusiaceae (*T. schomburgkii*), and Moraceae (*B. lactescens*) families. Leaf area index (LAI) reaches a maximum of 5.0 m^2/m^2 during the wet season and a minimum of 2.5 m^2/m^2 during the dry season (Sanches et al. 2008a). The soil is a quartzarenic neosol composed of ≈90 % sand, which has high porosity and drains within 4–7 days of rainfall events (Vourlitis et al. 2008).

Field measurements

Two different eddy covariance systems were used to measure *E* over the January 2000–2007 study period. Both systems were mounted in the direction of the mean wind at a height of 42 m above ground level, or 12–14 m above the forest canopy. The first system (January 2000–March 2005) consisted of a three-dimensional sonic anemometer-thermometer (SWS-211/3K, Applied Technologies Inc., Boulder, CO, USA) and an open-path infrared gas analyzer (NOAA-ATDD, Oak Ridge, TN, USA) to measure the mean and fluctuating quantities of wind speed and temperature and H_2O vapor, respectively (Vourlitis et al. 2001, 2002, 2004, 2005; Priante et al. 2004). Raw H_2O vapor fluctuations were outputted as mean voltages and converted to densities by multiplying by the requisite calibration constant (Leuning and Moncrieff 1990), and latent (Q_e) and sensible heat (Q_h) fluxes were computed following a coordinate rotation of the wind vectors (McMillen 1988). Fast response (10 Hz) fluxes were calculated and stored on a laptop computer as 30-min averages using a 200-s running mean and digital recursive filtering technique. Although longer time constants have been suggested to minimize errors in the estimation of low-frequency turbulent fluxes (Rannik and Vesala 1999), analysis of raw data using 200- and 800-s time constants suggests that the potential for underestimating of low-frequency turbulent flux was small (Ferreira 2004).

The second eddy covariance system (March 2005–January 2007) utilized a three-dimensional sonic anemometer-thermometer (CSAT-3, Campbell Scientific, Inc., Logan, UT, USA) and an open-path infrared gas analyzer (LI-7500, LI-COR, Inc. Lincoln, NE, USA) to measure the mean and fluctuating quantities of wind speed and temperature and

H_2O vapor, respectively (Vourlitis et al. 2008, 2011). Raw (10 Hz) data and 30-min average fluxes of Q_e and Q_h were stored and processed using a solid-state data logger (CR5000, Campbell Scientific, Inc., Logan, UT, USA). Average fluxes of Q_e and Q_h were calculated as the covariance between the fluctuations in vertical wind speed and H_2O vapor density and temperature, respectively, over a 30-min interval following a coordinate rotation of the wind vectors.

Sensors for both systems sampled and output data at 10 Hz. The H_2O vapor channel of the gas analyzers used for both systems was calibrated approximately monthly using a portable dew-point generator (LI-610, LI-COR, Inc. Lincoln, NE, USA). Water vapor flux for both measurement systems was corrected for the simultaneous fluctuations in heat (Webb et al. 1980). Unfortunately, both systems were not operational at the same time, so cross-comparison of the eddy covariance systems was not possible.

Net radiation was measured above the canopy (40 m above ground level) using a net radiometer (Q*7, REBS, Inc., Bellevue, WA, USA or NR-LITE, Kipp and Zonen, Bohemia, NY, USA). Soil heat flux was measured using heat flux transducers (n=2) buried approximately 2 cm into the surface litter layer (HFT-3.1, REBS, Inc., Bellevue, WA, USA). Air temperature and atmospheric water vapor density were measured at the top of the tower (42 m above ground level) using a thermohygrometer (HMP-35, Vaisala, Inc., Helsinki, Finland). Precipitation was measured at the top of the tower using a tipping-bucket rainfall gauge (TE-525; Texas Electronics, Inc., Dallas, TX, USA), and data gaps were filled with data obtained from a manual rain gauge that was read daily by personnel from the Fazenda Maracai located 5 km E of the study site. These data were highly correlated to data collected on-site (Vourlitis et al. 2008). Micrometeorological data were averaged every 30 min from observations made every 60 s and stored on a datalogger (CR5000, Campbell Scientific, Inc., Logan, UT, USA).

Gap-filling of E

Power system and/or sensor failure limited the amount of data collected from the eddy covariance system, and over the 7-year study period, the eddy covariance system was operational only 53 % of the time. However, the meteorological system used a separate power system and was operational more frequently than the eddy covariance system, and over the 7-year study period, the meteorological system was operational for 77 % of the time. Therefore, data collected from the more consistent meteorological measurements, along with the direct measurements of E from the eddy covariance system, were used to estimate E for the measurement period. Instantaneous (30-min average) rates of latent heat flux (Q_e) were calculated from micrometeorological data using the Priestley and Taylor (1972) equation,

$$Q_e = \alpha\left(s/s+\gamma\right)\left(Q^*-Q_g\right), \quad (1)$$

where α=the Priestley–Taylor coefficient, s=slope of the saturation vapor pressure vs. temperature curve at a given temperature, γ=psychrometric constant, and Q^* and Q_g are the net radiation and ground heat flux, respectively, measured from the meteorological sensors. The advantage of Eq. 1 is that Q_e is calculated using variables that are known to be important for driving spatial and temporal variations in Q_e (i.e., available energy and air and surface humidity), and few data are required to estimate the Q_e. However, the theoretical basis of α is unclear, and α can vary substantially depending on canopy roughness and surface water content (Xu and Singh 2000). Given a known Q_e, such as that measured from eddy covariance, estimates of α calibrated to local conditions of canopy roughness and surface moisture can be estimated for a given time period by rearranging Eq. 1 (Viswanadham et al. 1991; Vourlitis et al. 2002),

$$\alpha = Q_e/\left(\left(s/s+\gamma\right)\left(Q^*-Q_g\right)\right) \quad (2)$$

Using linear regression with the origin forced through zero, calibrated values of α were estimated for each month using Eq. 2 when eddy covariance measurements of Q_e were available, with the 30-min average Q_e measured from eddy covariance as the dependent variable and the 30-min average $(s/s+\gamma)(Q^*-Q_g)$ measured from the micrometeorological sensors as the independent variable (see for example, Fig. 2). When no eddy covariance data were available, values of α were interpolated for months before and after eddy covariance data were available, while longer gaps were filled using the mean variation approach (Falge et al. 2001) where values of α were estimated as the mean value for a given month.

Using calibrated values of α, daily estimates of E were calculated using Eq. 1, where $E=Q_e/\lambda$, and λ is the latent heat of vaporization. Daily estimates of E were averaged over weekly intervals, providing estimates of E for 77 % of all possible weeks. Missing values of E, which occurred when there were gaps in meteorological data, were estimated using auto-regressive, integrated moving average (ARIMA) models, which were fit to the E time series using an iterative Box–Jenkins approach (Edwards and Coull 1987).

Error analysis and estimation

Errors associated with the calibrated estimates of E (Eq. 1) were calculated assuming both random and systematic sources of error (Moncrieff et al. 1996). Random errors in E were

estimated as a function of the ±95 % confidence interval (±95 % CI) of α calculated by linear regression (Eq. 2). Systematic errors in E were estimated by assuming that all of the error associated with energy balance closure was due to a systematic error in the under-measurement of E from eddy covariance. This assumption is reasonable given that E is measured by two different sensors (i.e., sonic anemometer and an open-path gas analyzer) that have differences in sensitivity and stability, are spatially separated, and may not be perfectly synchronized (Burba 2013); however, we recognize that errors associated with energy balance closure may stem from a variety of sources including errors in the measurement of available energy and sensible heat flux (Wilson et al. 2002). Our eddy covariance systems have typically exhibited an energy balance closure of 78–92 % (Vourlitis et al. 2001, 2002, 2004, 2005, 2008, 2011; Priante et al. 2004). Using estimates of energy balance closure for each month, a new value of monthly α was recalculated (Eq. 2) after increasing the value of E to achieve perfect energy balance closure. The new value of α was then used to recalculate a daily value of E (Eq. 1) to reflect a systematic under-measurement of E. The difference between the estimates of E assuming full and normal energy balance closure was taken as the systematic error in E. The total error associated with the weekly estimate of E was then calculated as the sum of the random and systematic errors. On average, systematic errors accounted for 51 % of the total estimated error in E.

Long-term trends in regional climate

Climate data collected over a 16-year period from 1989 to 2005 consisting of total monthly rainfall and average monthly humidity and air temperature were obtained from the National Climatic Data Center (www.NCDC.gov) for 7 sites located within or adjacent to the 9–14° S transition zone of the southern Amazon Basin (Fig. 1; Table 1). Unfortunately, longer time series were not available for these sites because of an increase in the frequency of data gaps before and after this 16-year period. Data gaps were filled by calculating the composite average of a given variable across all sites and regressing the time series of a given site against the composite average. An inverse-distance weighting function (Isaaks and Srivastava 1989) was used to estimate the monthly climatology for the Sinop study site from 1989 to 2005.

Statistical analysis

Power spectral analysis was used to quantify the time scales of variance and elucidate the potential for cycles in the E and climate data (Platt and Denman 1975; Baldocchi et al. 2001). Following Baldocchi et al. (2001), Fourier transformation techniques were used to decompose the time series into a series of frequencies, and peaks in spectral density are observed as a function of frequency or period. Time series were differenced prior to Fourier transformation by subtracting each observation by the mean of the time series. The power

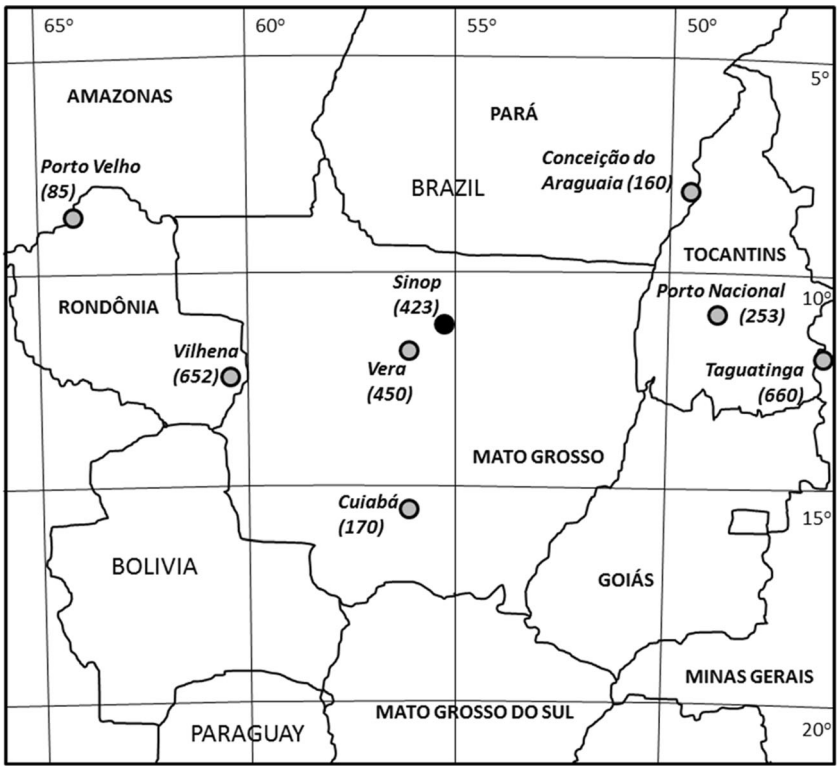

Fig. 1 Map of the study region with the state of Mato Grosso (*center*) and the Sinop, Mato Grosso study site (*black circle*). Also shown are the location and elevation of sites used to reconstruct the long-term (16 years) climate (*gray circles*) for the rainforest-savanna transition zone near the Sinop study site

Table 1 Characteristics of the sites used to reconstruct the long-term (1989–2005) regional changes in climate for the forest-transition zone of the SE Amazon Basin

WMO ID	Station name	Latitude (deg S)	Longitude (deg W)	Elevation (m)	Distance to Sinop (km)	Direction (deg)	Weighting
82861	Conceição do Araguaia	8° 15′	49° 17′	160	690	61	0.10
83361	Cuiabá	15° 33′	56° 07′	170	472	198	0.14
83064	Porto Nacional	10° 43′	48° 25′	253	690	82	0.10
82825	Porto Velho	8° 46′	63° 55′	85	1,054	295	0.06
83235	Taguatinga	12° 16′	46° 26′	660	910	96	0.07
83264	Vera	12° 12′	56° 30′	450	162	213	0.41
83208	Vilhena	12° 44′	60° 08′	652	563	258	0.12

Data include the World Meteorological Office identification, station name, latitude and longitude, elevation, distance and direction from the Sinop, Mato Grosso field site, and the weighting used to generate the average climate trend for Sinop, Mato Grosso. The weighting scheme was calculated as an inverse-distance weighting that calculated the ratio of the inverse distance of a given site divided by the sum of the inverse distances of all sites

spectral densities were normalized by their respective variances, so when plotted on a log–log scale, the area under the curve equaled unity (Baldocchi et al. 2001).

Temporal trends in E and local and regional climate variables (air temperature, vapor pressure, rainfall, and dry season duration) were assessed using ordinary linear regression (Fig. 2). A temporal trend was determined to be significantly different from zero if the mean (±95 % CI) slope did not encompass zero.

Results

Seasonal trends in α, E, and microclimate

There was a clear seasonal pattern in the Priestley–Taylor coefficient (α) where α was highest in May at the end of the wet season and lowest in September at the end of the dry season (Fig. 3). Values ranged from a maximum of 1.32 in May 2002, which exceeds the value of 1.26 for saturated surfaces (Priestley and Taylor 1972), to a minimum of 0.41 in September 2002 (Fig. 3; Supplementary data Table S1). Overall, α was on average (±95 % CI) 0.75±0.05, and the coefficient of determination of the linear regression (r^2) between the eddy covariance measurements of latent heat flux (Q_e) and the meteorological variables (Eq. 2) was 0.84 (range=0.62–0.92; Table S1).

Average weekly rates of E generally increased during the wet season in January and February and reached a peak in March–April; however, week-to-week and interannual variability was high (Fig. 4a). After the March–April peak, E declined during the dry season into September and increased only slightly into December even though there was adequate rainfall (Fig. 4a, c). The seasonal pattern of E was similar to the seasonal pattern in Q^* (Fig. 4b) with the exception that Q^* exhibited substantially less variability than E during the May–

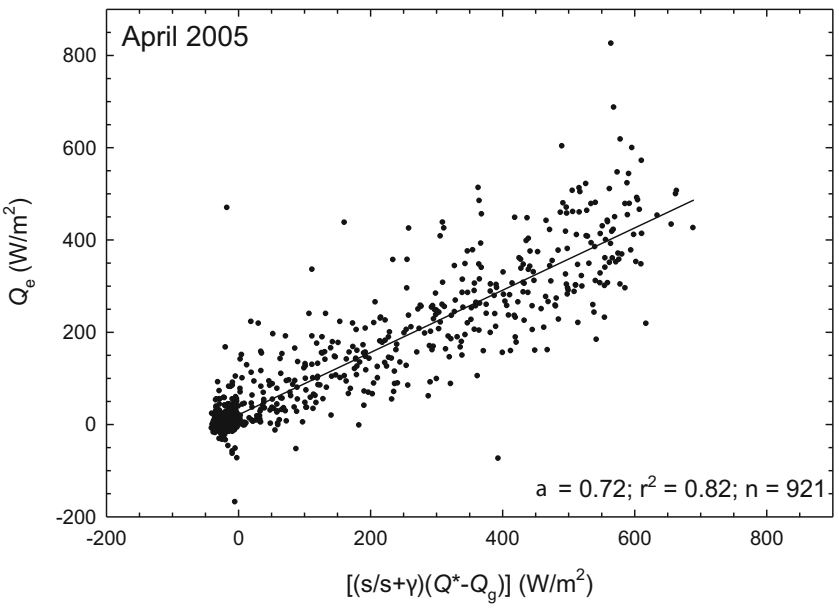

Fig. 2 An example of the linear regression method used to calculate the calibrated Priestley–Taylor coefficient α from eddy covariance measurements of latent heat flux (Q_e) and micrometeorological data consisting of temperature, net radiation (Q^*), and ground heat flux (Q_g) for April 2005. The slope of the regression corresponds to α with the regression forced through the origin (see Eq. 2). Also shown is the coefficient of determination (r^2) and the number of instantaneous (30-min average) values (n) used to estimate α

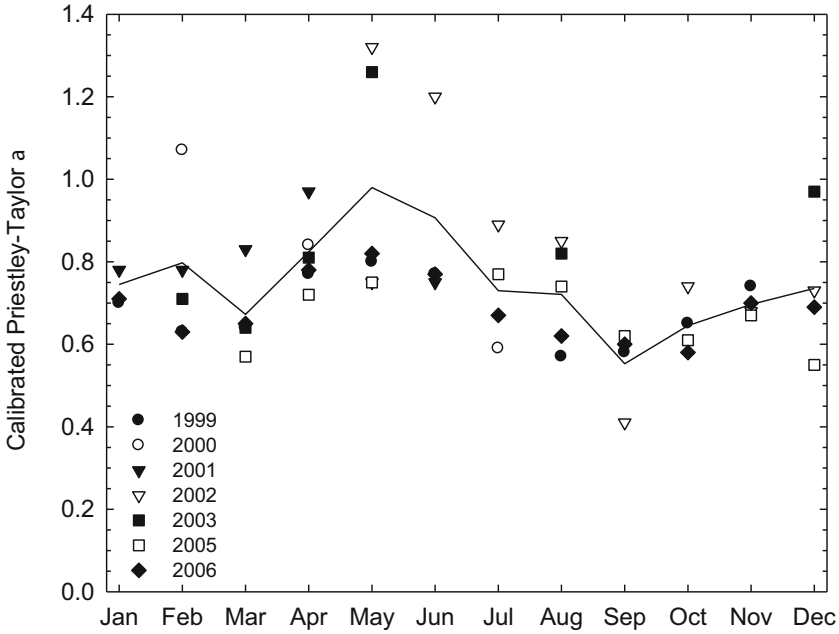

Fig. 3 Average monthly values of the calibrated Priestley–Taylor coefficient α calculated from eddy covariance measurements of latent heat flux (Q_e) and micrometeorological variables (Eq. 2). The *solid line* displays the interpolated values used when eddy covariance measurements of Q_e were not available

September dry season, and Q^* increased more than E during the October–December dry–wet season transition. Weekly variations in rainfall revealed a distinct wet season between October and April and a distinct dry season between May and September (Fig. 4c). During the wet season, week-to-week and interannual variations in rainfall were large, with some weeks experiencing up to 300 mm of rainfall and others experiencing no measureable rainfall, but during the dry season, there were extended periods when there was no measureable rainfall. Rapid increases and declines in rainfall were apparent during the dry–wet (September–October) and wet–dry (April–May) season transitions, respectively.

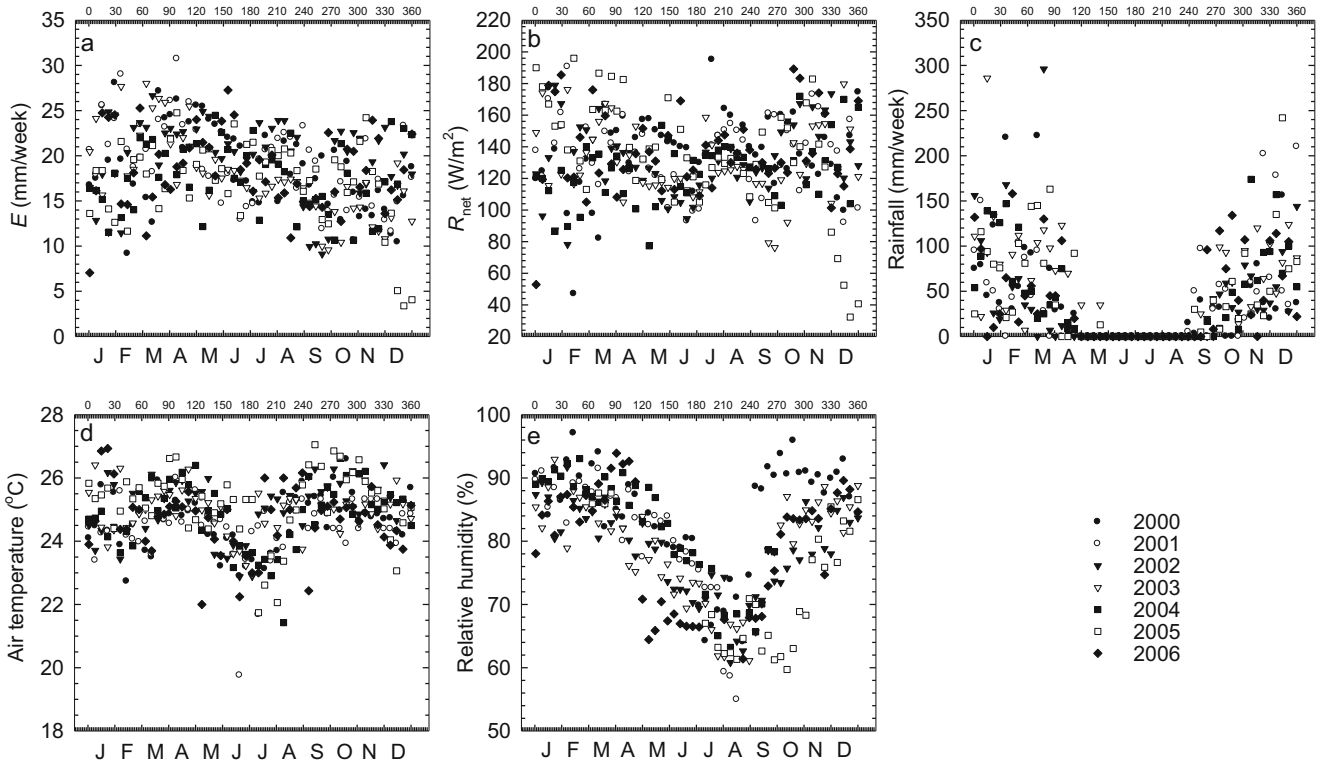

Fig. 4 **a** Average weekly evapotranspiration, **b** net radiation (Q^*), **c** total weekly rainfall, **d** average weekly air temperature, and (**e**) relative humidity as a function of day of the year (upper x-axis) and month (lower x-axis) for the January 2000–2007 study period

Seasonal variations in air temperature (Fig. 4d) and relative humidity (Fig. 4e) exhibited relatively less week-to-week and interannual variations compared with other meteorological variables, and on average, temperature and humidity were higher during the wet season and lower during the dry season.

Interannual trends in α, *E*, and microclimate

Weekly estimates of *E* for the 7-year study period varied substantially over time with a mean of 18.5 mm/week (2.6 mm/day) and a range of 3.4–30.7 mm/week (0.5–4.4 mm/day) (Fig. 5a; Supplementary data Table S2). Large temporal variations in *E* notwithstanding, our data indicate a small but statistically significant decline in *E* over time (Fig. 5a), and when calculated over an annual time scale (Table 2), *E* declined by on average (±95 % CI) 17.6± 12.0 mm/year (n=7 years; r^2=0.74; p<0.01) over the study period. The declining trend in *E* was not coincident with declines in local rainfall or net radiation, as temporal trends in these time series were not significantly different from zero (Fig. 5; Table 2). However, the decline in *E* was coincident with a significant increase in average weekly air temperature, with the average (±95 % CI) warming on the order of 0.001± 0.0009 °C/week, or 0.052 °C/year (Fig. 5c).

Power spectral densities for *E* (Fig. 6a), air temperature (Fig. 6b), and rainfall (Fig. 6c) exhibited peaks over 52-week cycles, indicating substantial annual variation in all of these variables. The temperature and rainfall time series exhibited a cycle on the order of a half year (20, 26 weeks), which reflects the periodicity associated with peaks in the wet and dry seasons (Fig. 4c, d). All three time series exhibited peaks in spectral density over 10–17-week cycles, which were coincident with seasonal climate peaks and transitions, and more rapid cycles occurred over 4–5- (Fig. 6a, c) and 2-week time scales (Fig. 6b), which were coincident with time scales of frontal activity.

Annual variations in rainfall were large and varied between 1,861 mm in 2002 and 2,645 mm in 2003 (Table 2). These years corresponded to an El Niño (2002)–La Niña (2003) cycle, which brought lower (2002) and higher than average (2003) rainfall to this portion of the Amazon Basin (Chen et al. 2010), but total annual *E* was remarkably similar (i.e., 1,008 and 942 mm, respectively) between these years despite the nearly 800-mm difference in annual rainfall. However, prior to El Niño (2000–2002), *E* was on average 1,011 mm/

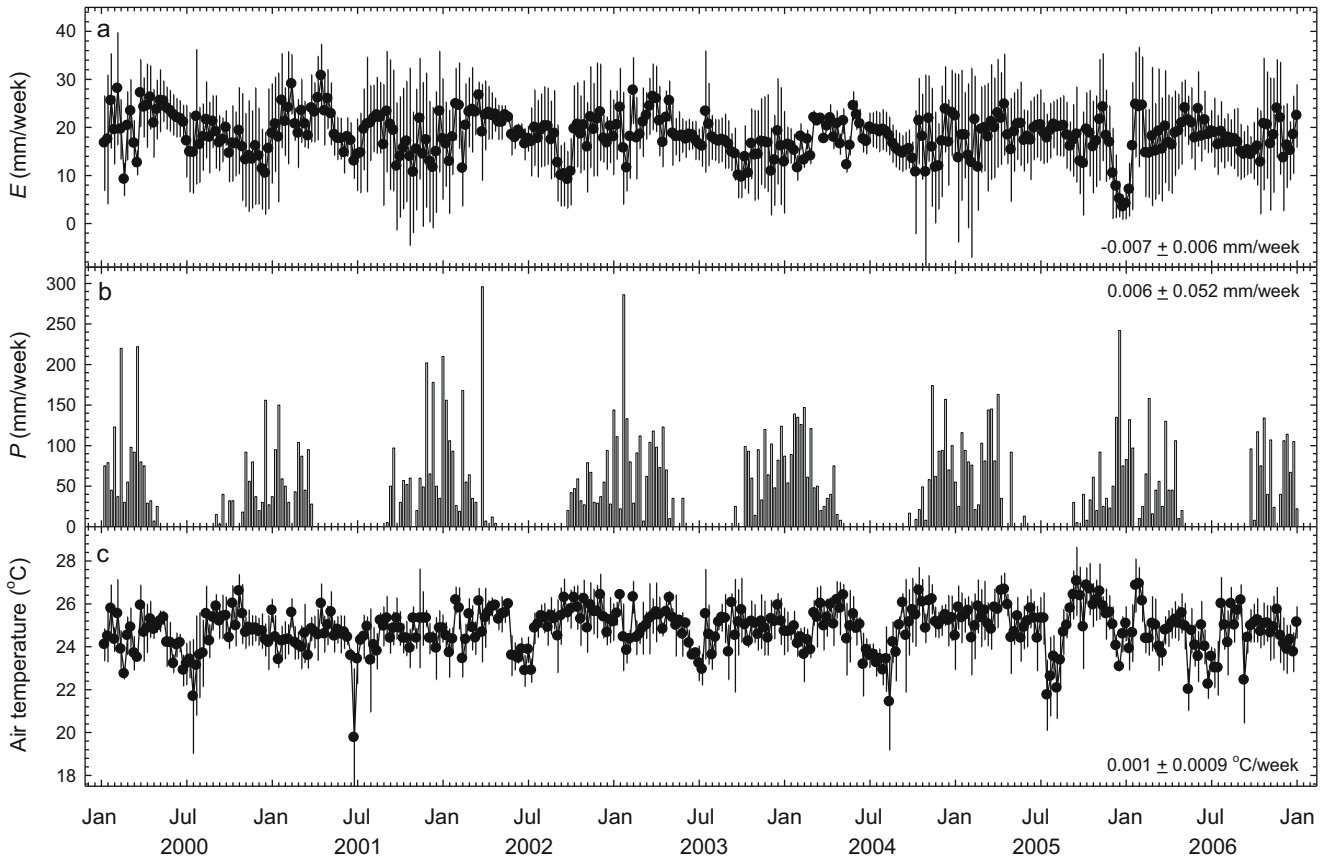

Fig. 5 **a** Average weekly evapotranspiration, **b** total weekly precipitation, and **c** average weekly air temperature for the January 2000–2007 study period. Also shown is the total error associated with estimating evapotranspiration (**a**), the standard deviation of mean weekly temperature (**c**), and the mean (±95 % CI) temporal trend calculated by ordinary linear regression

Table 2 Total annual precipitation and evapotranspiration (E), average annual temperature, relative humidity (RH), net radiation (R_{net}), the ratio of evapotranspiration to precipitation (E/P), and dry season duration from January 2000 to 2007. Also shown are the grand mean±1sd

Year	Rainfall (mm)	Dry season (weeks)	Temperature (°C)	RH (%)	R_{net} (W/m^2)	E (mm)	E/P
2000	1,999	26.0	24.6	84.5	137.1	1,009	0.50
2001	2,006	25.0	24.5	80.9	135.5	1,018	0.51
2002	1,861	31.0	25.0	78.3	131.9	1,008	0.54
2003	2,645	23.0	24.9	78.8	128.8	942	0.36
2004	2,155	28.0	24.8	81.2	126.1	934	0.43
2005	2,253	28.0	25.2	72.2	134.8	908	0.40
2006	2,040	22.0	24.7	79.3	136.3	942	0.46
Average	2,137	26.1	24.8	79.3	132.9	965	0.46
sd	256	3.1	0.3	3.8	4.1	44	0.07

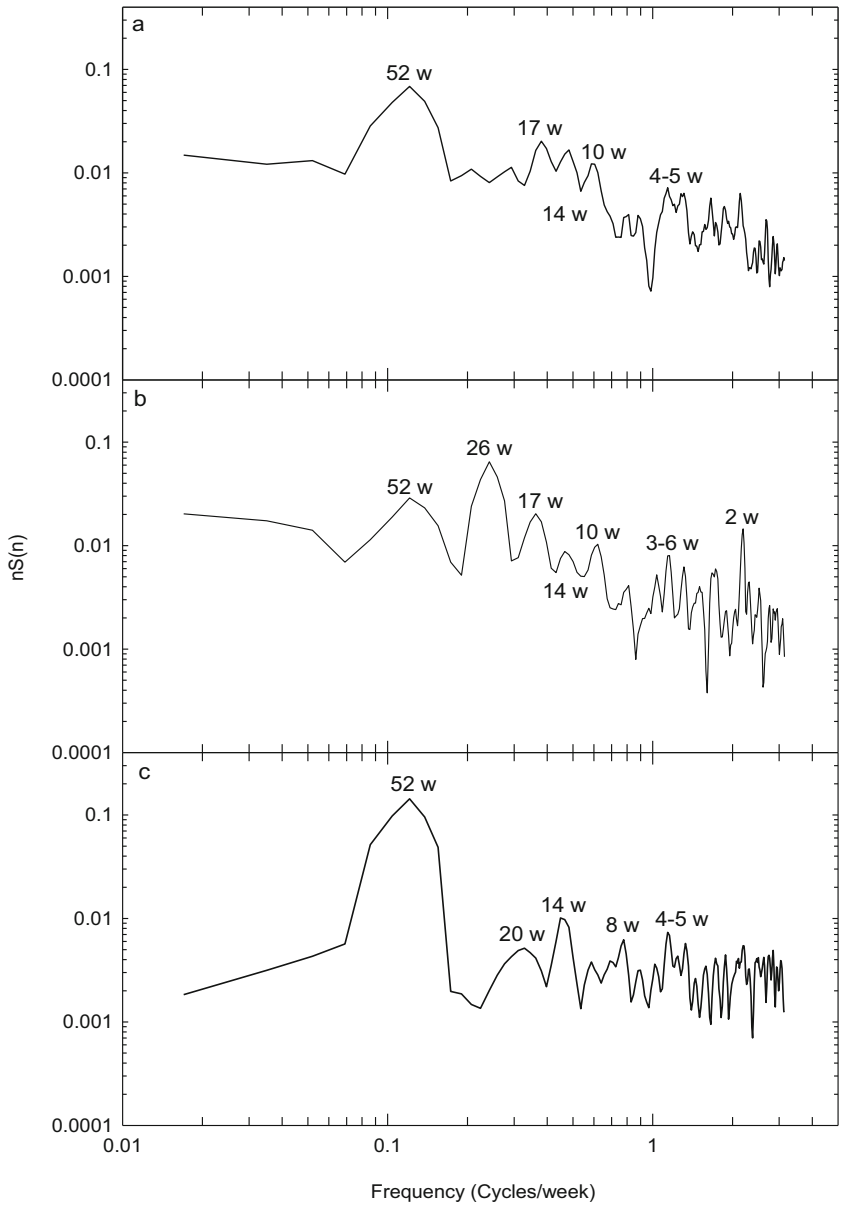

Fig. 6 Normalized power spectra of average weekly evapotranspiration (**a**), air temperature (**b**), and total weekly rainfall (**c**) for the January 2000–2007 study period. Numbers above peaks in spectral density correspond to the period (weeks/cycle) associated with each spectral peak. The power spectral densities were normalized by their respective variances so when plotted on a log–log scale, the area under the curve equaled unity

year and accounted for 52 % of the annual precipitation, while after (2003–2007), *E* was on average 931 mm/year and accounted for on average 41 % of the annual precipitation (Table 2). Results of a two-tailed *t* test (4 degrees of freedom) indicate that the values of *E* and *E*/*P* before and after the 2002 El Niño event were significantly different (*E*: $t=9.39$, $p<0.01$; *E*/*P*: $t=4.09$, $p<0.05$).

Long-term variations in climate for the forest-savanna transition

Climate records for locales within and/or adjacent to the 9–14° S forest-savanna transition zone ($n=7$ sites; Fig. 1) indicate that the recent local warming trend observed for the study site (Fig. 5c) was part of a longer, regional warming trend (Fig. 7a). Average monthly air temperature increased significantly over the 16-year period, with a weighted-average (±95 % CI) rate of warming for the Sinop region equal to 0.074±0.024 °C/year (Fig. 7a). Total monthly rainfall declined at five of the seven sites; however, temporal trends were not statistically significant (Fig. 7b). In contrast, atmospheric vapor pressure exhibited a significant decline (−0.008 ±0.005 kPa/year; Fig. 7c), while the length of the dry season, defined as the number of consecutive months with rainfall <50 mm, increased by 0.07±0.05 months/year (Fig. 7d). An inspection of the El Niño years of 1992–1993, 1998, and 2002 indicate an overall decline in rainfall and an increase in dry season length and temperature for these periods (Fig. 7).

Power spectral analysis indicates substantial variation over a 40–68-month (3.3–5.6 years) time scale for the air temperature time series, which may be indicative of El Niño-driven climate variations (Fig. 8a); however, no such cycle was apparent with the rainfall or atmospheric vapor pressure time series (Fig. 8b, c). Shorter cycles associated with annual

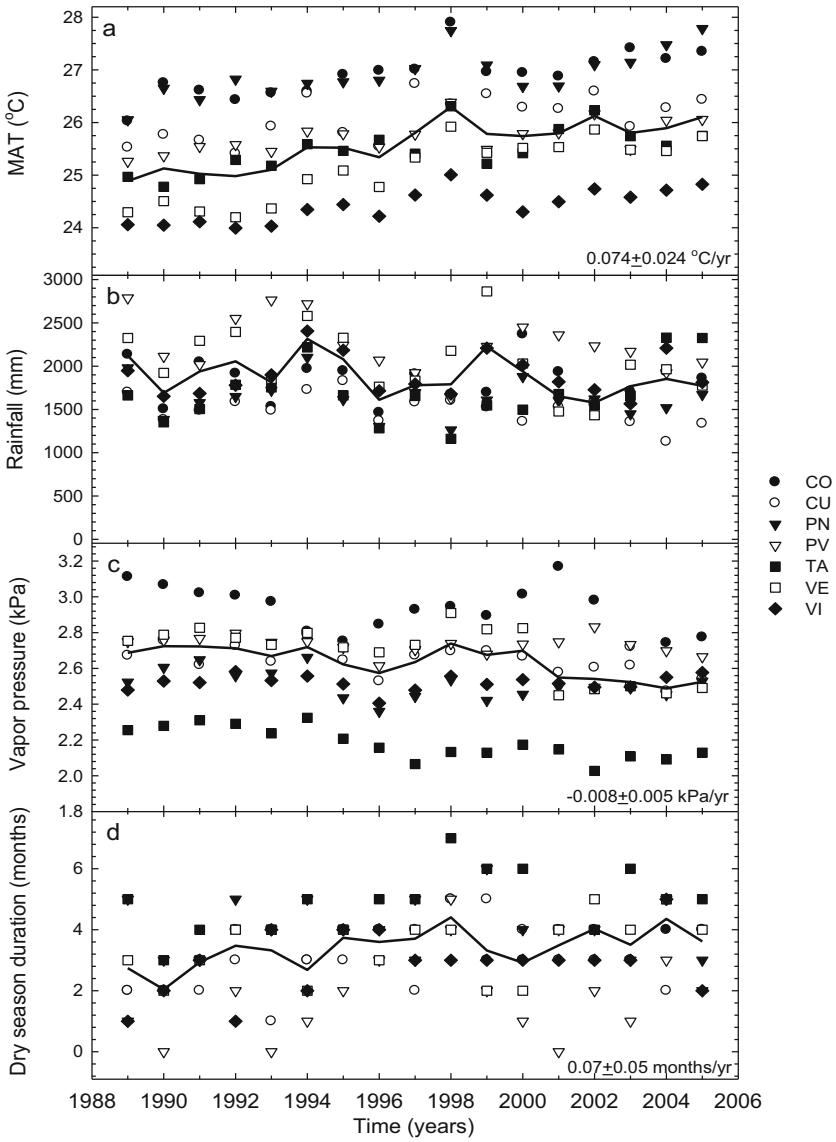

Fig. 7 **a** Mean annual temperature (MAT), **b** total annual precipitation, **c** atmospheric vapor pressure, and (**d**) dry season duration for 1989–2005 for sites located within or adjacent to the forest-savanna transition zone (9–14° S) of the SE Amazon Basin. Data are for Conceição do Araguaia (CO), Cuiabá (CU), Porto Nacional (PN), Porto Velho (PV), Taguatinga (TA), Vera (VE), and Vilhena (VI) and were acquired from the National Climate Data Center (www.NCDC.gov). The *solid line* represents an average for the Sinop, Mato Grosso region that was calculated from an inverse-distance weighting function

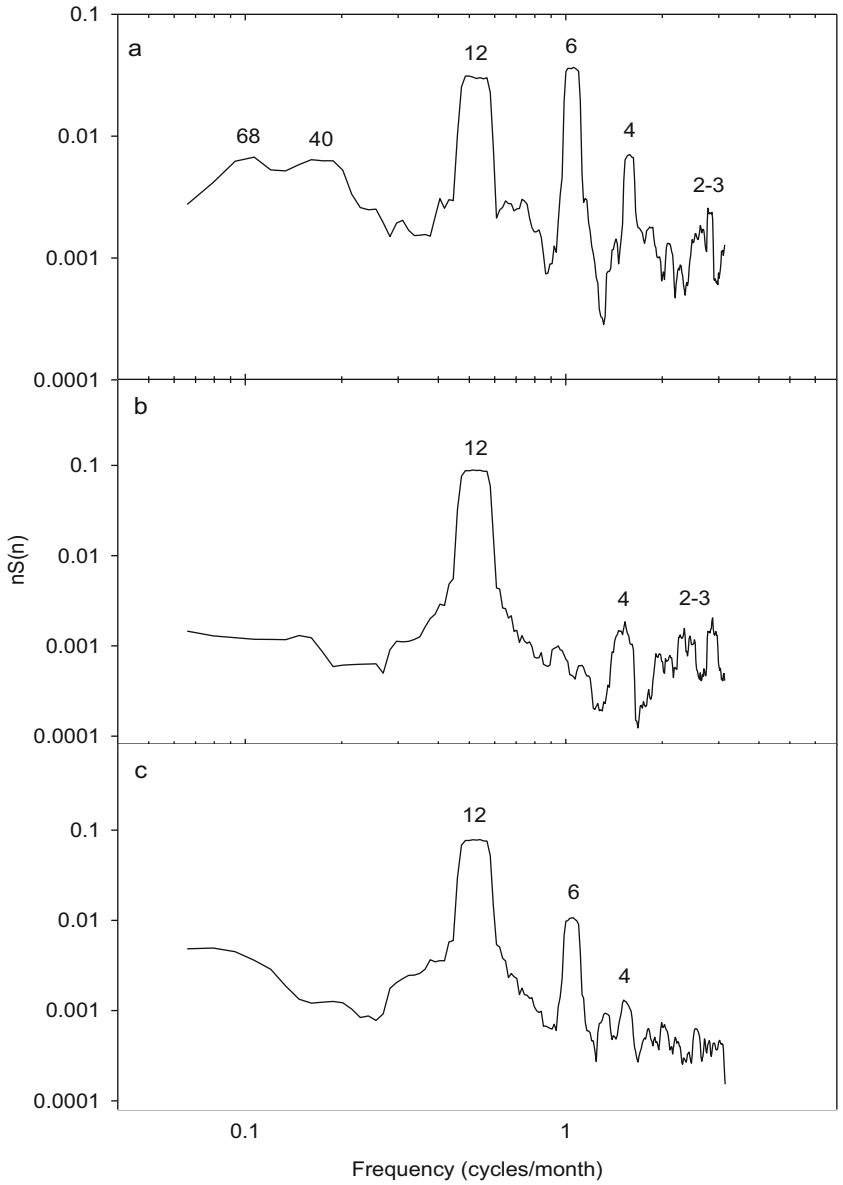

Fig. 8 Normalized power spectra of average monthly air temperature (**a**), total monthly rainfall (**b**), and average monthly atmospheric vapor pressure (**c**) for 1989–2005. Numbers above peaks in spectral density correspond to the period (months/cycle) associated with each spectral peak. The power spectral densities were normalized by their respective variances so when plotted on a log–log scale, the area under the curve equaled unity

(12 months), semiannual (6 months), and seasonal (2–4 months) time scales were also apparent in the regional temperature and vapor pressure time series, while total monthly rainfall displayed significant variation associated with annual (12 months) and seasonal (2–4 months) time scales only.

Discussion

Temporal patterns in *E* and local climate

Evapotranspiration (*E*) exhibited large seasonal variations that are consistent with those reported for other seasonal tropical forests or woodlands (von Randow et al. 2004; da Rocha et al. 2009; Vourlitis and da Rocha 2011; Rodrigues et al. 2013). However, seasonal patterns were not completely coincident with seasonal variations in net radiation (Fig. 4b), rainfall (Fig. 4c), temperature (Fig. 4d), or humidity (Fig. 4e), suggesting complex interactions between these, and other, variables. For example, net radiation (Q^*) was on average higher during the wet season but was also highly variable because of frequent cloud cover (Fig. 4b), which may act to limit rates of *E* when water availability is ample (Malhi et al. 2002; Vourlitis et al. 2005, 2008; da Rocha et al. 2009). During the dry season, high atmospheric demand for water vapor may favor high rates of *E* provided that trees are not limited by drought, and while tropical forest trees may have access to deep water (Nepstad et al. 1994; Hodnett et al. 1995; Vourlitis et al. 2008), declines in *E* are often observed in seasonally dry forests because of declines in stomatal conductance (Bucci et al. 2008; Sendall et al. 2009; Dalmagro et al. 2013) and/or LAI (Vourlitis et al. 2008). In the transitional forest studied here,

LAI reaches a minimum at the end of the dry season (Sanches et al. 2008a; Zeilhofer et al. 2011), which is coincident with the seasonal minimum in *E* (Fig. 4a), and because whole-forest transpiration is positively correlated with LAI (Vourlitis et al. 2008), the dry season decline in *E* is due in part to leaf shedding in response to seasonal drought. After the onset of rainfall in September, *E* may remain low because of lags between leaf area development and rainfall (Vourlitis et al. 2004; Meir and Grace 2005; Sanches et al. 2008b).

Spectral analysis revealed cycles in the *E* and local meteorology time series that occurred over a variety of time scales. Over annual time scales, the transitional forest exhibited significant interannual variation in rainfall and meteorology that affect LAI (Sanches et al. 2008a), litter production (Sanches et al. 2008b; Zeilhofer et al. 2011), net CO_2 exchange (Priante et al. 2004; Vourlitis et al. 2001, 2004, 2005, 2011), and *E* (Vourlitis et al. 2008) (Figs. 4a and 5). Air temperature and rainfall exhibited a semiannual cycle that reflected large seasonal variations in atmospheric circulation (i.e., location of the intertropical convergence zone) that are typical for this region (Machado et al. 2004). Over shorter time scales, 10–17-week cycles reflected more subtle seasonal climate states such as the seasonal peaks in temperature and rainfall and the transition periods between the wet and dry seasons (Machado et al. 2004), while cycles in temperature and moisture over shorter (2 weeks) time scales reflected cycles associated with frontal movement (Carvalho et al. 2002).

Our data also suggest a significant decline in *E* for the rainforest-savanna transition of northern Mato Grosso (Fig. 5a; Table 2). The magnitude of decline is consistent with regional-scale estimates of *E* during the same time period for the Amazon Basin (Jung et al. 2010) and the state of Mato Grosso (Lathuilliere et al. 2012) and with model estimates of tropical forest *E* in response to deforestation (Pongratz et al. 2006; Garcia-Carreras and Parker 2011; Costa and Pires 2010). The decline in *E* is also coincident with an increase in temperature of approximately 0.052 °C/year (Fig. 5c), which is comparable to the trend reported for SE Amazonia as a whole (Malhi and Wright 2005).

Even more striking was the change in *E* in response to the 2002 El Niño event, which caused a significant decline in terrestrial water storage (Chen et al. 2010). Rates of *E*, and the proportion of rainfall recycled to the atmosphere by *E*, were on average 90 mm and 11 % lower, respectively, after the 2002 El Niño event (Table 2), indicating significant, long-lasting changes in energy partitioning. While the actual mechanism for this decline is unknown, warming and drying during El Niño can cause changes in forest structure and function that may last for several years after the event (Saleska et al. 2003; Qian et al. 2008; Phillips et al. 2010). For example, stem and reproductive litter production for this forest, which are sensitive indicators of forest productivity and reproductive output (Mahli et al. 2004), declined significantly during the 2002 El Niño and recovered slowly thereafter (Sanches et al. 2008b). In addition, temporal trends in the MODIS-enhanced vegetation index (EVI) and the normalized difference vegetation index (NDVI) for this forest, which are sensitive to spatial and temporal variations in LAI (Zhao and Running 2010), exhibited a significant decline in response to the 2002 El Niño event (Zeilhofer et al. 2011). These data suggest that drought-induced forest structural changes led to a decline in *E* that lasted for several years after the event. In contrast, changes in *E* in response to the 2005 drought, which was more extreme in some parts of the Amazon Basin than the 2002 El Niño (Marengo et al. 2008), were negligible, but this might be due to the fact that precipitation was close to normal for this region despite higher temperatures and lower humidity (Table 2; Fig. 4d, e). However, it is noteworthy that the minimum value of E recorded during the study period (3.4 mm/week; Fig. 5a; Table S2) was observed during the wet season immediately following the 2005 drought event.

Long-term variations in climate for the forest-savanna transition zone

Our data suggest that the forest-savanna transition zone of northern Mato Grosso has experienced significant warming and drying since 1989 (Fig. 7). While trends in rainfall were equivocal (Fig. 7b), a decline in atmospheric vapor pressure (Fig. 7c) and an increase in the duration of the dry season (Fig. 7d) suggest that regional drying was associated with warming. An increase in the length of the dry season can potentially lead to an increase in drought stress, which will cause a decline in leaf photosynthesis and stomatal conductance (Sendall et al. 2009; Dalmagro et al. 2013), an increase tree mortality (Phillips et al. 2005), and presumably, a decline in *E* over time.

These time series also displayed significant variation over a variety of time scales (Fig. 8). For example, temperature varied significantly over 3.3–5.5-year cycles that are consistent with the return interval of El Niño (Potter et al. 2004; Malhi and Wright 2005). El Niño years of 1992–1993, 1998, and 2002 tended to be warmer than intervening years, which is consistent with trends observed for the SE Amazon Basin as a whole (Malhi and Wright 2005). Interestingly, there was no such periodicity with rainfall or atmospheric vapor pressure; however, there was also substantial intra and interannual variability in rainfall (Fig. 5c) and there is also a weaker correlation between El Niño and rainfall extremes for the Amazon Basin (Kane 1999).

The local warming trend (Fig. 5c) observed for the study site was consistent with the longer, regional trend (Fig. 7a), and both trends are consistent with observations and modeling studies that describe the climate response to land cover change. The savanna-forest transition region of northern Mato Grosso has experienced rapid rates of deforestation (Costa and Pires 2010), with 15 % of the forest and woodland converted to pasture and/or agriculture over the last 20 years, and as

much as 35 % over the last 30–40 years (Soares-Filho et al. 2006). Even more forested land area was likely degraded by land cover change (Laurance 2005). Higher temperatures associated with deforested surfaces can enhance convection, which can draw moist air from forested surfaces (Baidya Roy and Avssar 2002; Garcia-Carreras and Parker 2011). Over time, this localized warming and drying can reduce *E* of forest fragments (Pongratz et al. 2006; Costa and Pires 2010).

Unfortunately, there are no data available to directly link our observed decline in *E* with a longer-term, regional warming and drying associated with deforestation. The results described here may simply reflect a relatively short-term, local trend in *E* and climate that are more closely tied to natural climate variation (i.e., El Niño cycles) and independent of land cover change. Furthermore, the regional warming and drying reported here may be an artifact of the monitoring stations used in this analysis, possible heat-island effects associated with the measurement sites, the relatively short duration of the time series, and/or the limited availability of climate data for the region. These caveats notwithstanding, and assuming our results are general for this region, continued warming and drying are likely to lead to further declines in local, and presumably, regional *E*. Deforestation under the current "business as usual" scenario is expected to reduce semi-deciduous forest area by 80 % in 2050 (Soares-Filho et al. 2006). Thus, future land cover change may be expected to cause further declines in *E* for the rainforest-savanna transition zone of SE Amazon Basin.

Conclusions

We found that the meteorology and *E* of a semi-deciduous forest in the southern Amazon Basin varied over multiple time scales. Seasonal and annual rates of *E* were affected by variations in water availability and temperature, and in particular, rates of *E* were significantly affected by an El Niño episode that occurred in 2002. Prior to this event, annual *E* was on average 1,011 mm/year and accounted for 52 % of the annual rainfall, while after the El Niño event, annual *E* was 931 mm/year and accounted for 42 % of the annual rainfall. Our data also suggest that *E* declined significantly over the 7-year study period while air temperature significantly increased. The increase in local air temperature was consistent with a long-term (16 year), regional warming and drying trend, and while we cannot directly link these climate trends to the increase in deforestation that occurred in this region over the last several decades, our results are consistent with what is expected from deforestation. These results suggest that periodic drought and/or warming induced by El Niño, climate change, and/or deforestation will cause declines in *E* for the rainforest-savanna transition of the southeast Amazon Basin.

Acknowledgments This research was supported in part by the National Geographic Society, Committee for Research and Exploration, the National Science Foundation, Division of International Programs (OISE-0003778; IRES-0968245), and Division of Environmental Biology-Ecosystem Studies (DEB-0343964), and the CAPES-CNPq Projeto Ciência sem Fronteira (Science Without Borders) program. Additional support was provided by California State University, San Marcos (CSUSM), the Conselho Nacional de Desenvolvimento Científico e Tecnológico (CNPq), Universidade Federal de Mato Grosso (UFMT), the Fundação de Amparo à Pesquisa do Estado de Mato Grosso (FAPEMAT), the Sindicato das Indústrias Madeireiras do Norte de Mato Grosso (SINDUSMAD), the Coordenação de Aperfeiçoamento de Pessoal de Nível Superior (CAPES), Fundação de Promoção Social do Estado de Mato Grosso (PROSOL), Brasil Telecom, Corpo de Bombeiros do Estado de Mato Grosso, NASA-LBA and the Instituto Nacional de Pesquisas Espaciais (INPE).

References

Ackerly DD, Thomas WW, Ferreira CAC, Pirani JR (1989) The forest-cerrado transition zone in southern Amazonia: results of the 1985 Projecto Flora Amazônica Expedition to Mato Grosso. Brittonia 41: 113–128

Arris LL, Eagleson PS (1994) A water use model for locating the boreal/deciduous forest ecotone in eastern North America. Water Resour Res 30:1–9

Baidya Roy S, Avissar R (2002) Impact of land use/land cover change on regional hydrometeorology in Amazonia. J Geophys Res 107. doi: 10.1029/2000JD000266

Baldocchi D, Falge E, Wilson K (2001) A spectral analysis of biosphere–atmosphere trace gas flux densities and meteorological variables across hour to multi-year time scales. Agric For Met 107:1–27

Bucci SJ, Scholz FG, Goldstein G et al (2008) Controls on stand transpiration and soil water utilization along a tree density gradient in a Neotropical savanna. Agric For Met 148:839–849

Burba G (2013) Eddy covariance method for scientific, industrial, agricultural and regulatory applications. LI-COR Biosciences, Lincoln, p 345

Carvalho LMV, Jones C, Silva Dias MAF (2002) Intraseasonal large-scale circulations and mesoscale convective activity in tropical South America during the TRMM-LBA campaign. J Geophys Res 107(D20):4309. doi:10.1029/2001JD000745

Chen JL, Wilson CRF, Tapley BD (2010) The 2009 exceptional Amazon flood and interannual terrestrial water storage change observed by GRACE. Water Resources Research 46 (12). doi:10.1029/2010WR009383

Costa MH, Pires GF (2010) Effects of Amazon and Central Brazil deforestation scenarios on the duration of the dry season in the arc of deforestation. Int J Climatol 30:1970–1979

Costa MH, Botta A, Cardille JA (2003) Effects of large-scale changes in land cover on the discharge of the Tocantins River, Southeastern Amazonia. J Hydrol 283:206–217

Cramer W, Bondeau A, Schaphoff S, Lucht W, Smith B, Sitch S (2005) Twenty-first century atmospheric change and deforestation: potential impacts on tropical forests. In: Mahli Y, Phillips OL (eds) Tropical forests and global atmospheric change. Oxford University Press, Oxford, pp 17–30

da Rocha HR, Manzi AO, Cabral OM et al (2009) Patterns of water and heat flux across a biome gradient from tropical forest to savanna in Brazil. J Geophys Res-Biogeosci 114:G00B12. doi:10.1029/2007JG000640

Dalmagro HJ, Lobo FA, Vourlitis GL, Dalmolin ÂC, Antunes MZ Jr, Ortíz CER, Nogueira JS (2013) Photosynthetic parameters for two

invasive tree species of the Brazilian Pantanal in response to seasonal flooding. Photosynthetica 51:281–294. doi:10.1007/s11099-013-0024-3

Edwards D, Coull BC (1987) Autoregressive trend analysis: an example using long-term ecological data. Oikos 50:95–102

Falge E, Baldocchi D, Olson R et al (2001) Gap filling strategies for long term energy flux data sets. Ag For Met 107:71–77

Ferreira Filho J (2004) Análise de tempos de amostragem para cálculos de fluxos em sistemas de covariância de vórtices turbulentos, para floresta de transição do sudoeste da Amazônia. Dissertação de Mestrado em Física e Meio Ambiente, Universidade Federal de Mato Grosso, Cuiabá. 47 p

Garcia-Carreras L, Parker DJ (2011) How does local tropical deforestation affect rainfall? Geophys Res Lett 38:L19802. doi:10.1029/2011GL049099

Hasler N, Avissar R (2007) What controls evapotranspiration in the Amazon Basin? J Hydromet 8:380–395

Hodnett MG, Pimentel da Silva L, da Rocha HR, Cruz Senna R (1995) Seasonal soil water storage changes beneath central Amazonian rainforest and pasture. J Hydrol 170:233–254

Isaaks EH, Srivastava RM (1989) An introduction to applied geostatistics. Oxford University Press, New York, p 561

Jung M, Reichstein M, Ciais P et al (2010) Recent decline in the global land evapotranspiration trend due to limited moisture supply. Nature 467:951–954

Kane RP (1999) Rainfall extremes in some selected parts of central and South America: ENSO and other relationships reexamined. Int J Climatol 19:423–455

Lathuilliere MJ, Johnson MS, Donner SD (2012) Water use by terrestrial ecosystems: temporal variability in rainforest and agricultural contributions to evapotranspiration in Mato Grosso, Brazil. Environ Res Lett 7: 024024 (12 pp). doi:10.1088/1748-9326/7/2/024024

Laurance WF (2005) Forest-climate interactions in fragmented tropical landscapes. In: Mahli Y, Phillips OL (eds) Tropical forests and global atmospheric change. Oxford University Press, Oxford, pp 31–40

Leuning R, Moncrieff J (1990) Eddy covariance CO_2 flux measurements using open- and closed-path CO_2 analyzers: corrections for analyzer water vapor sensitivity and damping fluctuations in air sampling tubes. Bound Layer Met 53:63–76

Lorenzi H (2000) Avores Brasileiras, vol 1. Instituto Plantarum de Estudos da Flora, Ltd, Saõ Paulo

Lorenzi H (2002) Avores Brasileiras, vol 2. Instituto Plantarum de Estudos da Flora, Ltd, Saõ Paulo

Machado LAT, Laurent H, Dessay N, Miranda I (2004) Seasonal and diurnal variability of convection over the Amazonia: a comparison of different vegetation types and large scale forcing. Theor Appl Climatol 78:61–77

Malhi Y, Wright J (2005) Late twentieth-century patterns and trends in the climate of tropical forest regions. In: Mahli Y, Phillips OL (eds) Tropical forests and global atmospheric change. Oxford University Press, Oxford, pp 3–16

Malhi Y, Pegoraro E, Nobre A, Grace J, Culf A, Clement R (2002) Energy and water dynamics of a central Amazonian rain forest. J Geophys Res 107(D20):8061. doi:10.1029/2001JD000623

Malhi Y, Baker TR, Phillips OL, Almeida S, Alvarez E, Arroyo L, Chave J, Czimczik CI, Di Fiore A, Higuchi N, Killeen TJ, Laurance SG, Laurance WF, Lewis LL, Montoya LMM, Monteagudo A, Neill DA, Vargas PN, Patiño S, Pitman NCA, Quesada CA, Salomão R, Silva JNM, Lezama AT, Martinez RV, Terborgh J, Vinceti B, Lloyd J (2004) The above-ground coarse wood productivity of 104 Neotropical forest plots. Glob Change Biol 10:563–591

Marengo JA, Nobre CA, Tomasella J, Oyama MD, De Oliveira GS, De Oliveira R, Camargo H, Alves LM, Brown IF (2008) The drought of Amazonia in 2005. J Clim 21:495–516. doi:10.1175/2007JCLI1600.1

McMillen RT (1988) An eddy correlation technique with extended applicability to non-simple terrain. Bound Layer Met 43:231–245

Meir P, Grace J (2005) The effects of drought on tropical forest ecosystems. In: Mahli Y, Phillips OL (eds) Tropical forests and global atmospheric change. Oxford University Press, Oxford, pp 75–86

Moncrieff JB, Mahli Y, Leuning R (1996) The propagation of errors in long-term measurements of land-atmosphere fluxes of carbon dioxide and water. Glob Change Biol 2:231–240

Nepstad DC, de Carvalho CR, Davidson EA, Jipp PH, Lefebvre PA, Negreiros GH, da Silva ED, Stone TA, Trumbore SE, Vieira S (1994) The role of deep roots in the hydrological and carbon cycles of Amazonian forests and pastures. Nature 372:666–669

Phillips OL, Baker TR, Arroyo L et al (2005) Late twentieth-century patterns and trends in Amazon tree turnover. In: Mahli Y, Phillips OL (eds) Tropical forests and global atmospheric change. Oxford University Press, Oxford, pp 107–128

Phillips OL, van der Heijden G, Lewis SL, Lopez-Gonzalez G, Aragao LEOC, Lloyd J, Malhi Y, Monteagudo A, Almeida S, Alvarez Davila E, Amaral I, Andelman S, Andrade A, Arroyo L, Aymard G, Baker TR, Blanc L, Bonal D, de Oliveira ACA, Chao K-J, Cardozo ND, da Costa L, Feldpausch TR, Fisher JB, Fyllas NM, Freita MA, Galbraith D, Gloor E, Higuchi N, Honorio E, Jimenez E, Keeling H, Killeen TJ, Lovett JC, Meir P, Mendoza C, Morel A, Nunez Vargas P, Patino S, Peh KS-H, Pena Cruz A, Prieto A, Quesada CA, Ramırez F, Ramırez H, Rudas A, Salamao R, Schwarz M, Silva J, Silveira M, Ferry Slik JW, Sonké B, Thomas AS, Stropp J, Taplin JRD, Vasquez R, Vilanova E (2010) Drought–mortality relationships for tropical forests. New Phyt 187:631–646

Platt T, Denman KL (1975) Spectral analysis in ecology. Annu Rev Ecol Sys 6:189–210

Pongratz J, Bounoua L, DeFries RS, Anderson LO, Mauser W, Klink CA (2006) The impact of land cover change on surface energy and water balance in Mato Grosso, Brazil. Earth Interactions 10: Paper No. 19, pp 17

Potter C, Klooster S, Steinbach M, Tan PN, Kumar V, Shekhar S, Carvalho CR (2004) Understanding global teleconnections of climate to regional model estimates of Amazon ecosystem carbon fluxes. Glob Change Biol 10:693–703

Priante Filho N, Vourlitis GL, Hayashi MMS et al (2004) Comparison of the mass and energy exchange of a pasture and a mature transitional tropical forest of the southern Amazon Basin during a seasonal transition. Glob Change Biol 10:863–876

Priestley CHB, Taylor RJ (1972) On the assessment of surface heat flux and evaporation using large-scale parameters. Mon Weather Rev 100:81–92

Qian H, Joseph R, Zeng N (2008) Response of the terrestrial carbon cycle to the El Niño-Southern Oscillation. Tellus 60B:537–550

Rannik Ü, Vesala T (1999) Autoregressive filtering versus linear detrending in estimation of fluxes by the eddy covariance method. Bound Layer Met 91:259–280

Rodrigues TR, de Paulo SR, Novais JWZ, Curado LFA, Nogueira JS, de Oliveira RG, Lobo FA, Vourlitis GL (2013) Temporal patterns of energy balance for a Brazilian tropical savanna under contrasting seasonal conditions. Int J Atm Sci 2013: Article ID 326010, 9 pages. doi:10.1155/2013/326010

Rodrigues TR, Vourlitis GL, Lobo FA, Oliveira RG, Nogueira JS (2014) Seasonal variation in energy balance and canopy conductance for a tropical savanna ecosystem of south-central Mato Grosso, Brazil. J Geophys R-Biogeosci 119:1–13. doi:10.1002/2013JG002472

Saleska SR, Miller SD, Matross DM et al (2003) Carbon in Amazon forests: unexpected seasonal fluxes and disturbance-induced losses. Science 302:1554–1557

Sanches L, Andrade NRL, Nogueira JS, Biudes MS, Vourlitis GL (2008a) Índice de área foliar em floresta de transição Amazonia cerrado em diferentes médotos de estimative. Revista de Ciência e Natura 30: 57–69

Sanches L, Valentini CMA, Borges Pinto O Jr, Nogueira JS, Vourlitis GL, Biudes MS, da Silva CJ, Bambi P, Lobo FA (2008b) Seasonal and interannual litter dynamics of a tropical semideciduous forest of the southern Amazon Basin, Brazil. J Geophys Res-Biogeosci 113, G04007. doi:10.1029/2007JG000593

Sendall MM, Vourlitis GL, Lobo FA (2009) Seasonal variation in the maximum rate of leaf gas exchange of canopy and understory tree species in an Amazonian semi-deciduous forest. Braz J Plant Phys 21:65–74

Soares-Filho BS, Nepstad DC, Curran LM, Cerqueira GC, Garcia RA, Ramos CA, Voll E, McDonald A, Lefebvre P, Schlesinger P (2006) Modelling conservation in the Amazon basin. Nature 440:520–523

Viswanadham Y, Silva Filho VP, Andre RGB (1991) The Priestley-Taylor parameter alpha for the Amazon forest. Forest Ecol Man 38:211–225

von Randow C, Manzi AO, Kruijt B, de Oliveira PJ, Zanchi FB, Silva RL, Hodnett MG, Gash JHC, Elbers JA, Waterloo MJ, Cardoso FL, Kabat P (2004) Comparative measurements and seasonal variations in energy and carbon exchange over forest and pasture in South West Amazonia. Theor Appl Climatol 78:5–26

Vourlitis GL, da Rocha HR (2011) Flux dynamics in the Cerrado and Cerrado-forest transition of Brazil. In: Hill MJ, Hanan NP (eds) Ecosystem function in global savannas: measurement and modeling at landscape to global scales. CRC, Inc, Boca Raton, pp 97–116

Vourlitis GL, Priante-Filho N, Hayashi MMS, Nogueira JS, Caseiro FT, Campelo JH Jr (2001) Seasonal variations in the net ecosystem CO_2 exchange of a mature Amazonian tropical transitional forest (cerradão). Funct Ecol 15:388–395

Vourlitis GL, Priante-Filho N, Hayashi MMS, Nogueira JS, Caseiro FT, Campelo JH Jr (2002) Seasonal variations in the evapotranspiration of a transitional tropical forest of Mato Grosso, Brazil. Water Resour Res 38:6

Vourlitis GL, Priante-Filho N, Hayashi MMS, Nogueira JS, Caseiro FT, Raiter F, Campelo JH Jr (2004) The role of seasonal variations in meteorology on the net CO_2 exchange of a Brazilian transitional tropical forest. Ecol Appl 14:S89–S100

Vourlitis GL, Nogueira JS, Priante-Filho N, Hoeger W, Raiter F, Biudes MS, Arruda JC, Capistrano VB, Faria JB, Lobo FA (2005) The sensitivity of diel CO_2 and H_2O vapor exchange of a tropical transitional forest to seasonal variation in meteorology and water availability. Earth Interactions 9:9–027

Vourlitis GL, Nogueira JS, Lobo FA, Sendall KM, Faria JLB, Dias CAA, Andrade NRL (2008) Energy balance and canopy conductance of a tropical semi-deciduous forest of the southern Amazon Basin. Water Resour Res 44, W03412. doi:10.1029/2006WR005526

Vourlitis GL, Lobo FA, Zeilhofer Z, Nogueira JS (2011) Temporal patterns of net CO_2 exchange for a tropical semideciduous forest of the southern Amazon Basin. J Geophys Res 116:G03029. doi:10.1029/2010JG001524

Webb EK, Pearman GI, Leuning R (1980) Corrections of flux measurements for density effects due to heat and water vapor transfer. Quart J Royal Meteor Soc 106:85–100

Wilson K et al (2002) Energy balance closure at FLUXNET sites. Agric For Met 113:223–243

Xu CY, Singh VP (2000) Evaluation and generalization of radiation-based methods for calculating evaporation. Hydro Proc 14:339–349

Zeilhofer P, Sanches L, Vourlitis GL, Andrade NRL (2011) Seasonal variations in litter production and its relation with MODIS vegetation indices in a semi-deciduous forest of Mato Grosso. Rem Sens Lett 3:1–9

Zhao M, Running SW (2010) Drought-induced reduction in global terrestrial net primary production from 2000 through 2009. Science 329:940–943